DOI: 10.1002/cmdc.201300533

Insight into the Functional and Structural Properties of 3-Arylcoumarin as an Interesting Scaffold in Monoamine Oxidase B Inhibition

Maria João Matos,*[a] Santiago Vilar,[a, b] Verónica García-Morales,[c] Nicholas P. Tatonetti,[b] Eugenio Uriarte,[a] Lourdes Santana,[a] and Dolores Viña[c]

The design, synthesis, pharmacological evaluation, and theoretical studies of a new series of halogenated 3-arylcoumarins were carried out with the aim of finding new structural and biological features. This series displays several alkyl, hydroxy, halogen, and/or alkoxy groups in both benzene rings of the 3-arylcoumarin scaffold. Most of the compounds studied show high affinity and selectivity for the human monoamine oxidase B (hMAO-B) isoenzyme, with IC_{50} values in the low nanomolar and picomolar range. Most of the evaluated compounds display higher MAO-B inhibitory activity and selectivity than selegiline (the reference compound). Coumarin **12** (3-(3-bromophenyl)-6-methylcoumarin) is the most active compound (IC_{50} = 134 pM), being 140-fold more active than selegiline and showing the highest specificity for hMAO-B. To better understand the structure–activity relationships, docking experiments were carried out on human monoamine oxidase (A and B) structures. Finally, the prediction of passive blood–brain partitioning, based on in silico derived physicochemical descriptors, was performed.

Introduction

Neurological diseases are considered as one of the important challenges in medicine because of the complexity, frequency of occurrence, and progressive development of these pathologies. Among these are the neurodegenerative disorders, such as Alzheimer's disease (AD) and Parkinson's disease (PD).[1,2] Their treatment still relies largely on replacing the missing dopamine (DA) without any targeting. L-DOPA, a DA prodrug, and drugs modifying the DA levels, such as dopaminic receptor agonists, muscarinic receptor agonists, catechol-*O*-methyltransferase (COMT) inhibitors, and selective monoamine oxidase type B inhibitors (MAOI-B) are commonly used to treat neurodegenerative diseases.[1–4] Moreover, MAOI-B, such as selegiline, show neuroprotective effects mediated by a pathway that is unrelated to the MAO inhibition.[5] Novel strategies to treat PD also focus on the formation of α-synuclein fibrils and the different possibilities to maintain the native protein by considering chaperone activity,[6] fibril proteolysis through autophagic systems,[7] and pathways of phosphorylation.[8]

MAO is an important flavin-containing enzyme, which catalyzes the oxidative deamination of monoamines[9] and is located in the outer mitochondrial membrane of neurons and other cells.[10] These enzymes are responsible for catalyzing the oxidative deamination of neurotransmitters and dietary amines, to regulate the intracellular levels of biogenic amines in the brain and the peripheral tissues.[11] Therefore, they play an important role in the inactivation of neurotransmitters and are often targeted when dysregulation of neurotransmitter levels occurs, as is the case for neurodegenerative disorders. The physiological properties determine the clinical interest of MAOI. MAOI-A (for example, clorgyline and moclobemide) are used in the treatment of depression and anxiety,[12] whereas MAOI-B (such as selegiline and rasagiline) have been applied to PD therapy (Figure 1).[13,14]

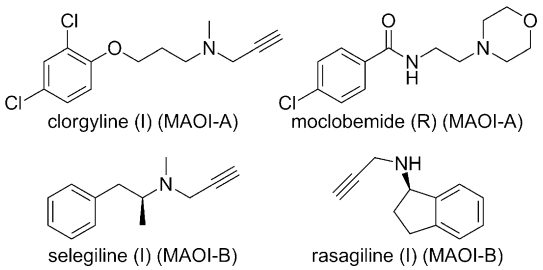

Figure 1. Chemical structures of MAOI-A (clorgyline and moclobemide) and MAOI-B (selegiline and rasagiline). I: irreversible, R: reversible.

In recent years, interest in selective hMAOI-B has significantly intensified because of the discovery that expression levels of this isoenzyme in neuronal tissue increase fourfold with age. This results in an increase of DA metabolism, as well as of the

[a] *Dr. M. J. Matos, Dr. S. Vilar, Prof. E. Uriarte, Prof. L. Santana*
Department of Organic Chemistry, Faculty of Pharmacy
University of Santiago de Compostela
15782 Santiago de Compostela (Spain)
E-mail: mariacmatos@gmail.com

[b] *Dr. S. Vilar, Dr. N. P. Tatonetti*
Department of Biomedical Informatics
Columbia University Medical Center, New York, NY 10032 (USA)

[c] *Dr. V. García-Morales, Prof. D. Viña*
Department of Pharmacology, CIMUS
University of Santiago de Compostela
15782 Santiago de Compostela (Spain)

production of hydrogen peroxide (H_2O_2). This fact could cause oxidative stress and may play a relevant role in the etiology of neurodegenerative diseases.[15] This research has resulted in a significant number of compounds with different structural scaffolds.[16,17] Additionally, the description of the crystal structure of the two MAO isoforms by Binda and co-workers has provided relevant information about the selective interactions and the pharmacophoric requirements needed for the design of potent and selective inhibitors.[18–22]

The presence of MAO in the brain cells means that MAOIs must be able to reach and cross the blood–brain barrier (BBB), which prevents the access of polar molecules to the brain. The distribution of compounds between the blood and brain is a very important consideration for new drug candidates. The prediction of passive blood–brain partitioning based on in silico derived physicochemical descriptors is an interesting tool.[23] Due to the issues described above, in the last few years, a broad consensus has been reached concerning the necessity for the research of new, more potent, and less toxic MAO-B selective inhibitors.

Coumarin is a natural product that can be found in the roots, leaves, flowers, or fruits of various families of angiosperms, such as *Apiaceae*, *Rutaceae*, *Asteraceae*, and *Umbelliferae*. Derivatives of this benzopyrone are of pharmaceutical interest because they have shown different biological activities. Work has been done that describes the coumarins as anticancer, anti-inflammatory, antimicrobial, cardioprotective, vasorelaxant, and antioxidant agents.[24] Therefore, the coumarin nucleus emerged in the 1990s as a promising scaffold for MAO inhibitors.[25] Structure–selectivity relationship studies about coumarin derivatives suggested that the selectivity was mainly determined by the nature of the linkage between the coumarin and the lipophilic aryl groups.[26] Furthermore, several coumarins showing significant MAO inhibitory activity (Figure 2) have been reported. Some of them have been suggested as potential drugs against neurodegenerative diseases.[27]

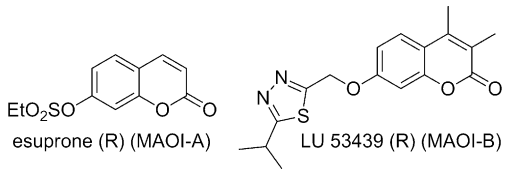

Figure 2. Structures of known coumarin-based MAOIs (esuprone and LU53439).

Our research group has been able to present 3-arylcoumarins (coumarin–stilbene hybrids; Figure 3) that show a high selectivity and affinity to the MAO-B isoenzyme.[28–37] These results encouraged us to synthesize and study the MAO inhibitory activity of new analogues, in which a variety of groups with different sizes or different electronic and lipophilic properties were introduced in both aromatic rings. Our intention is to clarify the influence of the substitution pattern on the MAO inhibitory activity and selectivity of the 3-arylcoumarin skeleton.

To analyze the structure requirements for the MAO activity shown by our compounds, we carried out docking experiments on models based on hMAO-A and hMAO-B. After considering the interesting preliminary results, our research group is still looking for more active and selective MAOIs.

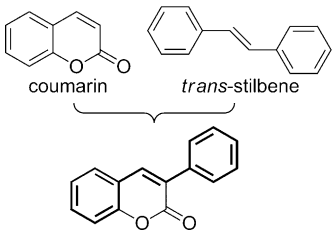

Figure 3. General chemical structure of the synthesized stilbene–coumarin hybrid scaffold.

Results

Chemistry

The coumarin derivatives **1**–**25** were efficiently synthesized according to the protocol outlined in Scheme 1. The detailed chemical structures of the compounds are organized in Table 1. The general reaction conditions and the compound characterizations are described below in the Experimental Section.

Perkin condensation of different *ortho*-hydroxybenzaldehydes with the appropriate arylacetic acid, by using *N*,*N*′-dicyclohexylcarbodiimide (DCC) as a dehydrating agent,[38–40] afforded the 3-arylcoumarins **1**–**3**, **5**–**8**, and **11**–**15**.[28,34,41] Treatment of 4-(methoxyphenyl)-6-methylcoumarin (**7**) and 3-(methoxyphenyl)-6-methylcoumarin (**8**)[40] with *N*-bromosuccinimide (NBS) in CCl_4 heated at reflux, by using 2,2′-azobisisobutyronitrile (AIBN) as a catalyst,[34] afforded the bromomethoxy derivatives **9** and **10**,[40] respectively. In addition, compounds **4**, **16**, and **17** were obtained by acidic hydrolysis of the respective methoxy derivatives **3**, **14**, and **15**, by using hydriodic acid (57%) in the presence of acetic acid and acetic anhydride.[39] Finally, the Williamson reaction of hydroxycoumarins **16** and **17** with chloroacetone, 2-chloroacetyl chloride, or cyclopentyl bromide[40] gave the corresponding ethers **18**–**20** and **21**–**23**, respectively. Due to their reactivity, compounds **20** and **23** were converted into **24** and **25** in presence of H_2O.

Pharmacology: in vitro inhibition of MAO

The biological evaluation of the test drugs on hMAO activity was investigated by measuring their effects on the production of hydrogen peroxide (H_2O_2) from *p*-tyramine (a common substrate for hMAO-A and hMAO-B), by using the Amplex Red MAO assay kit (Molecular Probes Inc., Eugene, OR, USA) and microsomal MAO isoforms prepared from insect cells (BTI-TN-5B1-4) infected with recombinant baculovirus containing complementary DNA (cDNA) inserts for hMAO-A or hMAO-B (Sigma–Aldrich Química S.A., Alcobendas, Spain).[42] The pro-

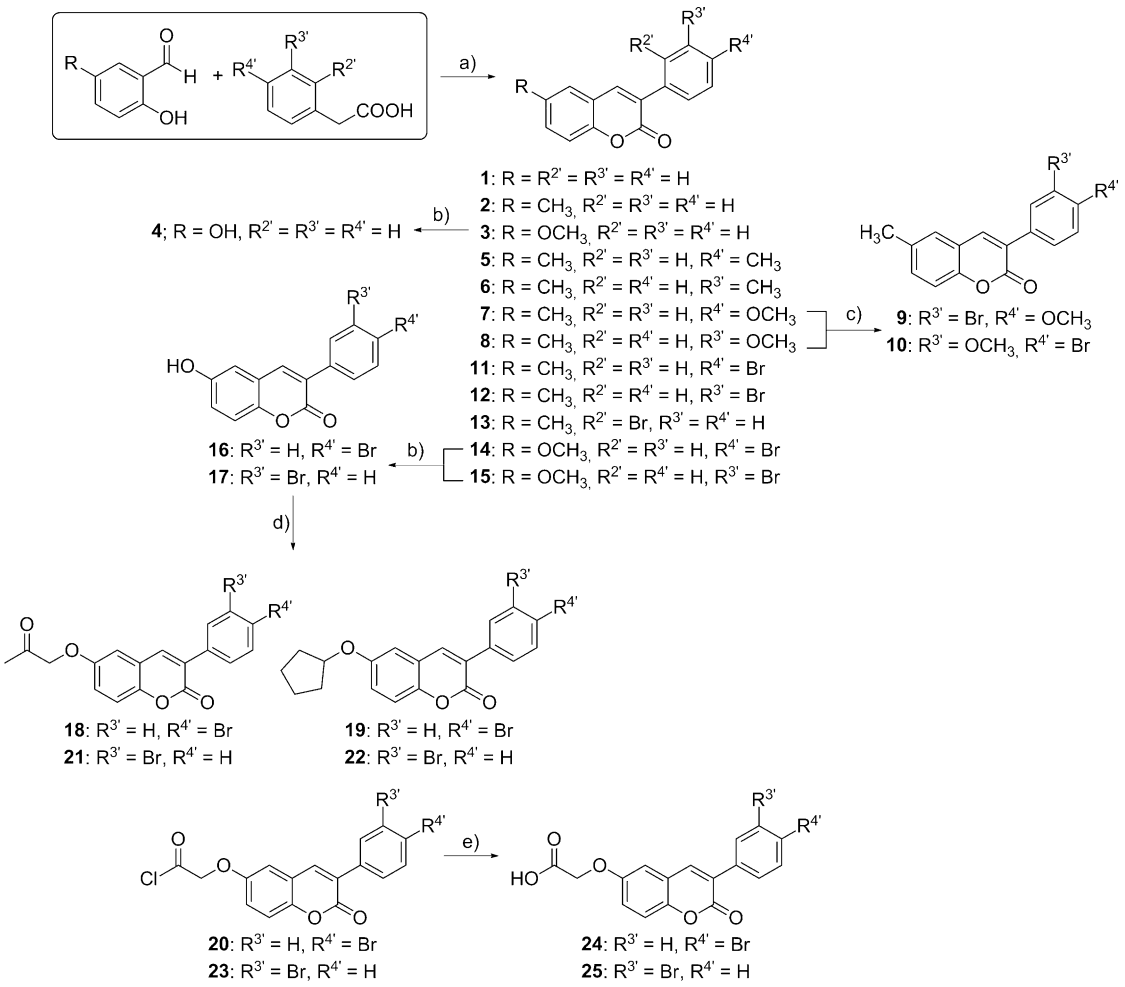

Scheme 1. *Reagents and conditions*: a) DCC, DMSO, 110 °C, 24 h, 60–83%; b) HI, AcOH, Ac_2O, reflux, 3 h, 80–89%; c) NBS, AIBN, CCl_4, reflux, 18 h, 41–51%; d) chloroacetone or cyclopentyl bromide or 2-chloroacetyl chloride, K_2CO_3, acetone, reflux, 16–24 h, 63–83%; e) $H_2O \approx 100$%. DCC: *N*,*N*′-dicyclohexylcarbodiimide; DMSO: dimethylsulfoxide; NBS: *N*-bromosuccinimide; AIBN: 2,2′-azobisisobutyronitrile; CCl_4: carbon tetrachloride.

duction of H_2O_2 catalyzed by the two MAO isoforms can be detected by using 10-acetyl-3,7-dihydroxyphenoxazine (Amplex Red reagent), a nonfluorescent and highly sensitive probe that reacts with H_2O_2 in the presence of horseradish peroxidase to produce a fluorescent product, resorufin. The new compounds and reference inhibitors were unable to react directly with the Amplex Red reagent, which indicates that these drugs do not interfere with the measurements. On the other hand, in our experiments and under our experimental conditions, hMAO-A displayed a Michaelis constant (K_M) equal to 457.17 ± 38.62 μM and a maximum reaction velocity (V_{max}) with the control group of 185.67 ± 12.06 nmol *p*-tyramine min^{-1} mg protein^{-1}, whereas hMAO-B showed a K_M value of 220.33 ± 32.80 μM and a V_{max} value of 24.32 ± 1.97 nmol *p*-tyramine min^{-1} mg protein^{-1} ($n = 5$). Most of the tested compounds concentration-dependently inhibited this enzymatic control activity (Table 1).

Reversibility experiments were performed to evaluate the type of inhibition for derivative **12**, the most active compound in the series (Table 2). An effective dilution method was used,[43] and selegiline (irreversible inhibitor) and isatin (reversible inhibitor) were taken are standards.[44]

To further examine the binding mode of **12** to MAO-B, the possibility that **12** acts as a competitive inhibitor of this enzyme was explored. For this purpose, Lineweaver–Burk plots were constructed for the inhibition of MAO-B by **12**. The initial catalytic rates of MAO-B were measured at five different concentrations (10–1000 μM) of the substrate, *p*-tyramine. These measurements were carried out in the absence and presence of four different concentrations of **12** (0.05–10 nM). The Lineweaver–Burk plots obtained in this manner are shown in Figure 4. The results show that the sets of Lineweaver–Burk plots constructed for the inhibition of MAO-B have a linear trend intersecting at the *x* axis. This indicates that the inhibition of the MAO-B enzyme by **12** is noncompetitive and thus provides further support that **12** is a reversible MAO-B inhibitor.

Prediction of passive blood–brain partitioning

Compounds designed to be effective in the central nervous system (CNS) should be able to cross the BBB to reach the therapeutic target. It has been shown that compounds with

Table 1. Structure and in vitro hMAO-A and hMAO-B inhibitory activity of the synthesized derivatives **1**–**25** and the reference compound selegiline.

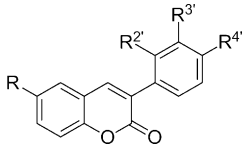

Compd	R	$R^{2'}$	$R^{3'}$	$R^{4'}$	IC_{50} [nM][a] hMAO-A	hMAO-B	SI[b]
1	H	H	H	H	–[c]	11810 ± 800	> 8.5[d]
2	CH_3	H	H	H	–[c]	283.75 ± 19.90	> 352[d]
3	OCH_3	H	H	H	–[c]	413.25 ± 60.50	> 242[d]
4	OH	H	H	H	29890 ± 2020	3390 ± 230	8.8
5	CH_3	H	H	CH_3	–[c]	0.31 ± 0.02	> 333333[d]
6	CH_3	H	CH_3	H	–[e]	15.01 ± 0.83	> 6667[d]
7	CH_3	H	H	OCH_3	–[c]	13.05 ± 0.90	> 7663[d]
8	CH_3	H	OCH_3	H	–[c]	0.80 ± 0.05	> 125000[d]
9	CH_3	H	Br	OCH_3	–[c]	0.74 ± 0.02	> 135870[d]
10	CH_3	H	OCH_3	Br	–[c]	3.25 ± 0.17	> 31250[d]
11	CH_3	H	H	Br	–[e]	0.387 ± 0.026	> 258371[d]
12	CH_3	H	Br	H	–[c]	0.134 ± 0.009	> 746045[d]
13	CH_3	Br	H	H	–[c]	4340 ± 290	> 23[d]
14	OCH_3	H	H	Br	–[c]	0.32 ± 0.017	> 312500[d]
15	OCH_3	H	Br	H	–[c]	0.65 ± 0.035	> 153846[d]
16	OH	H	H	Br	12830 ± 660	32.0 ± 1.7	387
17	OH	H	Br	H	–[c]	8.0 ± 0.43	> 12500[d]
18	$C_3H_5O_2$	H	H	Br	–[c]	–[e]	–
19	C_5H_9O	H	H	Br	–[c]	7020 ± 380	> 14[d]
20	$C_2H_2O_2Cl$	H	H	Br	n.e.	n.e.	–
21	$C_3H_5O_2$	H	Br	H	–[c]	1480 ± 79	> 68[d]
22	C_5H_9O	H	Br	H	44290 ± 2400	1790 ± 96	25
23	$C_2H_2O_2Cl$	H	Br	H	n.e.	n.e.	–
24	$C_2H_3O_3$	H	H	Br	12660 ± 840	7.01 ± 0.47	1809
25	$C_2H_3O_3$	H	Br	H	–[c]	2.4 ± 0.14	> 37037[d]
seleg.	–	–	–	–	67250 ± 1020	19.60 ± 0.86	3431

[a] Values are the mean ± SEM from five experiments ($n = 5$); n.e.: not evaluated due to compound instability. [b] Selectivity index: MAO-B selectivity ratios $[IC_{50(MAO\text{-}A)}]/[IC_{50(MAO\text{-}B)}]$ for the inhibitory effects of both new compounds and reference inhibitors. [c] Inactive at 100 μM (highest concentration tested); at higher concentrations, the compounds precipitate. [d] Values obtained under the assumption that the corresponding IC_{50} value against MAO-A is the highest concentration tested (100 μM). [e] 100 μM inhibits the corresponding hMAO activity by ~40–45%; at higher concentrations, the compounds precipitate.

a logarithm of the ratio of the concentration of the compound in the brain and in the blood (log *BB*) of less than −1 are poorly distributed in the brain, whereas molecules with log *BB* > 0.3 can readily cross the BBB.[45,46] The distribution of compounds **1**–**25** between the blood and the brain was calculated through a discriminant equation extracted from a model recently published.[23] The equation discriminates between compounds with log *BB* values by using a cutoff of 0.3 (see Equation (1) in the Experimental Section section). The topological polar surface area (TPSA) and the logarithm of the octanol/water partition coefficient (log $P_{(o/w)}$) were calculated and their values were substituted into Equation (1). If the result in the equation is greater than 0, the compounds are predicted to have log *BB* ≥ 0.3, which means that the compounds readily cross the BBB.[45,46] If the result is less than 0, the compounds could still cross the BBB but with log *BB* < 0.3. The majority of the compounds were predicted to cross the BBB (Table 3). To better understand the overall properties of the described compounds, the theoretical prediction of other absorption, distribution, metabolism and excretion (ADME) properties (molecular weight, log *S* value, number of hydrogen donors and acceptors) of all of the studied compounds (**1**–**25**) was carried out and is presented in Table 3.

Table 2. Reversibility results of hMAO-B inhibition by derivative **12** and reference inhibitors.

Compd	Concentration	Slope [%][a]
12	0.150 nM	26.53 ± 1.77
selegiline	20 nM	8.51 ± 0.62
isatin	33 μM	67.80 ± 7.54

[a] Measured as fluorescence in atomic units over time. Percentage values represent the mean ± SEM of five experiments ($n = 5$) relative to control; data show recovery of hMAO-B activity after dilution.

Molecular docking studies in hMAO-B

Molecular docking calculations were performed to detect the most likely ligand–protein conformation for the 3-arylcoumarin

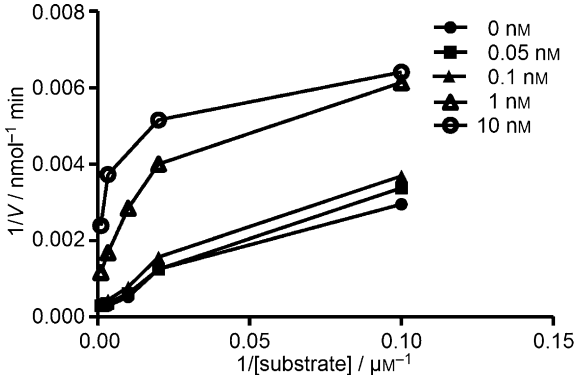

Figure 4. Lineweaver–Burk plots of the catalytic rates of human MAO-B in the absence (●) and presence of various concentrations of **12**: 0.05 nM (■), 0.1 nM (▲), 1 nM (△) and 10 nM (○). The catalytic rates (*V*) are expressed as nmol product formed min^{-1} (mg protein)$^{-1}$.

Table 3. Molecular descriptors (TPSA and log $P_{(o/w)}$) included in Equation (1), log *BB* prediction for the compounds included in the study, and other calculated theoretical descriptors.[a]

Compd	log $P_{(o/w)}$	TPSA	Value in Eq. (1)	log $BB \geq 0.3$	Other descriptors						
					a_acc	a_don	lip_druglike	lip_violation	log *S*	m.r.	M_r [Da]
1	3.881	26.300	0.927	+	1	0	1	0	−4.55	6.63	222.24
2	4.216	26.300	1.100	+	1	0	1	0	−5.02	7.08	236.27
3	3.874	35.530	0.668	+	2	0	1	0	−4.60	7.27	252.27
4	3.61	46.530	0.227	+	2	1	1	0	−4.19	6.76	238.24
5	4.514	26.300	1.254	+	1	0	1	0	−5.50	7.52	250.30
6	4.551	26.300	1.273	+	1	0	1	0	−5.50	7.52	250.30
7	4.172	35.530	0.822	+	2	0	1	0	−5.07	7.72	266.30
8	4.209	35.530	0.841	+	2	0	1	0	−5.07	7.72	266.30
9	5.005	35.530	1.252	+	2	0	1	0	−6.16	8.47	345.19
10	5.005	35.530	1.252	+	2	0	1	0	−6.16	8.47	345.19
11	5.014	26.300	1.512	+	1	0	1	0	−6.11	7.82	315.17
12	5.051	26.300	1.531	+	1	0	1	0	−6.11	7.82	315.17
13	5.012	26.300	1.511	+	1	0	1	0	−6.11	7.82	315.17
14	4.672	35.530	1.080	+	2	0	1	0	−5.69	8.01	331.16
15	4.709	35.530	1.099	+	2	0	1	0	−5.69	8.01	331.16
16	4.408	46.530	0.639	+	2	1	1	0	−5.28	7.50	317.14
17	4.445	46.530	0.658	+	2	1	1	0	−5.28	7.50	317.14
18	4.353	52.600	0.442	+	3	0	1	0	−6.03	9.02	373.20
19	6.209	35.530	1.873	+	2	0	1	1	−6.65	9.67	385.26
20	5.077	52.600	0.816	+	3	0	1	0	−6.84	9.06	393.62
21	4.39	52.600	0.462	+	3	0	1	0	−6.03	9.02	373.20
22	6.246	35.530	1.892	+	2	0	1	1	−6.65	9.67	385.26
23	5.114	52.600	0.835	+	3	0	1	0	−6.84	9.06	393.62
24	4.298	75.660	−0.225	−	2	0	1	0	−5.95	8.63	374.17
25	4.335	75.660	−0.206	−	2	0	1	0	−5.95	8.63	374.17

[a] log $P_{(o/w)}$: log of the octanol/water partition coefficient; TPSA: topological polar surface area; *a*_acc: number of H-bond acceptor atoms; *a*_don: number of H-bond donor atoms; lip_druglike = 1 if lip_violation < 2; lip_violation: number of violations of Lipinski's rule; log *S*: log of the aqueous solubility [M]; m.r.: molecular refractivity.

derivatives. By following a similar docking protocol recently published,[31] the crystal structure of the hMAO-B in complex with 7-(3-chlorobenzyl)oxycoumarin-4-carboxaldehyde (**C17**; Protein Data Bank (PDB): 2V60)[47] was used to dock the compounds under study. Water molecules were deleted, with the exception of the water molecule establishing a hydrogen bond with the crystallographic ligand. The docking simulations were carried out by using the QM-polarized ligand docking module in the Schrödinger package (see the Experimental Section for a detailed description). We performed a re-docking validation by using the co-crystallized **C17** (PDB: 2V60), as well as the crystallized ligands from other hMAO-B structures (PDB: 1OJ9, 1OJA, 1OJD, 2BK3, 2V5Z, 2V61, 2XFN, 3PO7, and 4A79).[48] The root-mean-square deviation (RMSD) of the heavy-atom coordinates between the calculated and crystallized poses was evaluated. The RMSD showed a value of 0.26 for the coumarin derivative **C17** in the hMAO-B 2V60 structure (Table 4 and Figure 5 a).

Table 4. RMSD values for the most stable poses calculated through QM-polarized docking with different co-crystallized ligands for hMAO-B (re-docking validation).

PDB code	RMSD	PDB code	RMSD
2V60	0.26	2V5Z	1.45
2XFN	0.77	2BK3	1.51
1OJ9	0.85	1OJA	1.90
1OJD	1.29	3PO7	2.66
2V61	1.38	4A79	2.68

Once the protocol was validated, we also carried out molecular docking calculations for the compounds of the synthesized series in the hMAO-B. Two of the most active compounds with substitutions at position 6 of the coumarin ring and *meta* or *para* positions in the 3-aryl ring were considered to be representative of the study (compounds **12** and **14**, Figure 5 b–d). The most favorable docking poses according to the energy score (E_{model}) were retrieved for all of the compounds. As was reported previously for this type of compound,[31–35] docking simulations in hMAO-B showed that the coumarin ring is oriented toward the bottom of the binding pocket in the majority of the docked coumarin derivatives. This fact showed the preference of this type of compound to adopt the described binding conformation (Figure 5). The phenyl ring in the benzopyrone system interacts with the flavin adenine dinucleotide (FAD) cofactor, Tyr60, Tyr398, Tyr435, and Phe343 through van der Waals and hydrophobic interactions. The 3-aryl fragment is directed toward the hydrophobic area in the entrance cavity, which establishes hydrophobic and van der Waals interactions mainly with residues Trp119, Leu164, Leu167, Phe168, Ile199, and Ile316 for compound **12** (the best compound of

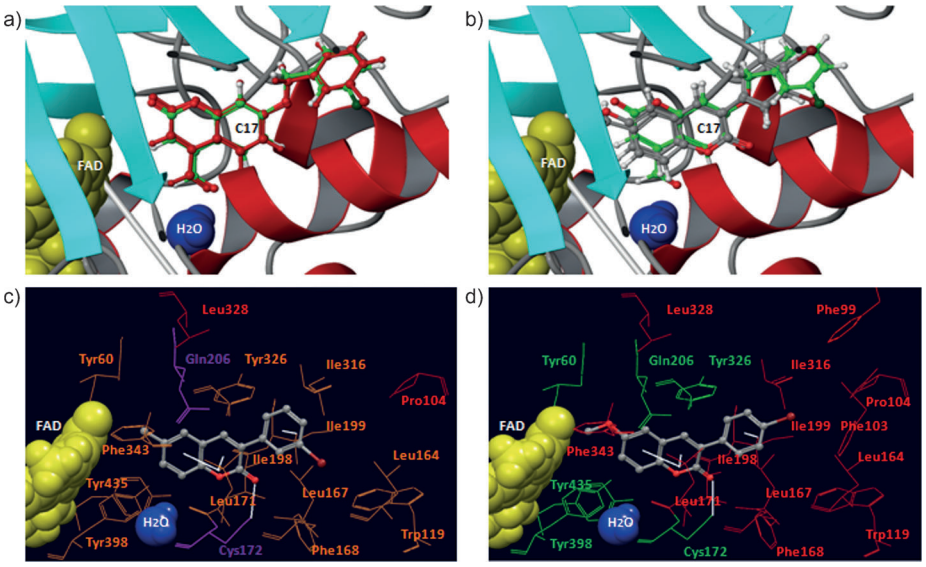

Figure 5. a) Comparison of the co-crystallized ligand **C17** (colored by element, green carbon atoms) in the crystal hMAO-B (PDB: 2V60) and the most stable pose retrieved by the docking calculation (red). The FAD cofactor is colored in yellow and the water molecule is in blue. b) Comparison of the most stable binding modes for compounds **12** and **14** (colored by element, gray carbon atoms) against the co-crystallized compound **C17** in the crystal hMAO-B (colored by element, green carbon atoms). c) Analysis of the most stable pose of compound **12** into the hMAO-B pocket. The hydrogen bond between Cys172 and the oxygen atom in the carbonyl group and the arene-H interactions with Leu171 and Ile199 are represented in white. Gln206 and Cys172 (violet) establish van der Waals interactions with the ligand. Leu328 and Pro104 (red) interact with compound **12** through hydrophobic forces. Residues that establish both hydrophobic and van der Waals interactions with the ligand are colored in orange. d) The most stable binding mode for compound **14** in hMAO-B. The hydrogen bond between Cys172 and the coumarin and the arene-H interactions are represented in white. The binding pocket is colored according to the residue property: the hydrophobic residues are colored in red and the hydrophilic residues are colored in green.

the presented series). The analysis of the binding mode for compounds **12** and **14** also showed that the ligand conformations are stabilized by a hydrogen bond between Cys172 and the oxygen atom in the carbonyl group of the coumarin ring. However, the H-bond angle is not optimum due to the fact that Cys172 also interacts through an intramolecular hydrogen bond with Phe168. Protein structure minimization by using the Prime module[49] optimized the hydrogen position and showed the cited hydrogen bond. In both compounds, Leu171 and Ile199 establish an arene-H interaction with the coumarin ring and the 3-aryl ring, respectively. The ligands also establish Coulomb interactions with the FAD cofactor and some residues, such as Glu84, Phe103, Leu171, Ile198, Ile199, Tyr326, and Tyr398. This fact supports the usefulness of the described protocol to analyze the binding mode of this type of coumarin derivative. However, the most stable ligand conformation could be highly dependent on the nature of the substituents in the 3-aryl ring, as well as the coumarin nucleus.

In this article, we also studied hMAO selectivity by using in silico evidence. We used the hMAO-A crystal structure (PDB: 2Z5X) to dock compounds **11** and **12**. Water molecules within 5 Å from the co-crystallized ligand were retained in the calculation. The RMSD between the theoretical and the crystallized conformations for the ligand harmine was 0.49 Å. Compound **12** was placed in a similar area to the co-crystallized ligand (Figure 6a). However, unlike the harmine ligand, the pose for compound **12** determined by docking did not show any H-bond contacts with any water molecules. This fact could explain the difference in hMAO-A activity between the compounds. A similar pose was found for compound **11** (Figure 6b). Moreover, to further study the hMAO-A activity, compound **24** was also investigated by docking. No water molecules were retained in the cavity because of the larger size of the compound. The docking pose is in agreement with the previous calculation (Figure 6b). However, the oxyacetic acid chain at position 6 is placed deeply in the cavity. The carboxylate oxygen atom replaced a water molecule and established a hydrogen bond with Tyr197, which could stabilize the ligand conformation (Figure 6b). However, this conformation would have to displace some water molecules present in the crystal structure that establish an important H-bond network with the protein, and this process could be energetically unfavorable and limiting to the ligand binding potential.

We also analyzed binding energy values extracted from the docking calculations. The docking showed better affinities for the hMAO-B isoenzyme. The different ligand–protein complexes were optimized by using the Prime module.[49] The molecular mechanics with generalized Born and surface area solvation (MM-GBSA) free energy of binding for the new synthesized compounds was calibrated with experimental pIC_{50} values through linear regression ($r = 0.24$ and $r = 0.43$ for hMAO-A and hMAO-B, respectively). Table 5 shows the MAO-A/B predicted pIC_{50} values for the most active compounds.

Discussion

All of the described coumarins in this report (compounds **1**–**25**) were efficiently synthesized and evaluated for their ability to inhibit the A and B isoforms of hMAO. The corresponding IC_{50} values and hMAO-B selectivity ratios, $[IC_{50\,(MAO\text{-}A)}]/[IC_{50\,(MAO\text{-}B)}]$, are shown in Table 1. The chemical structures of the newly designed compounds, as well as the biological and docking results, can help us with an interesting structure–activity relationship (SAR) study. A theoretical prediction, based on in silico derived physicochemical descriptors, of the BBB crossing was carried out, and the results also encouraged us to explore the potential of this chemical family as drug candidates. The ma-

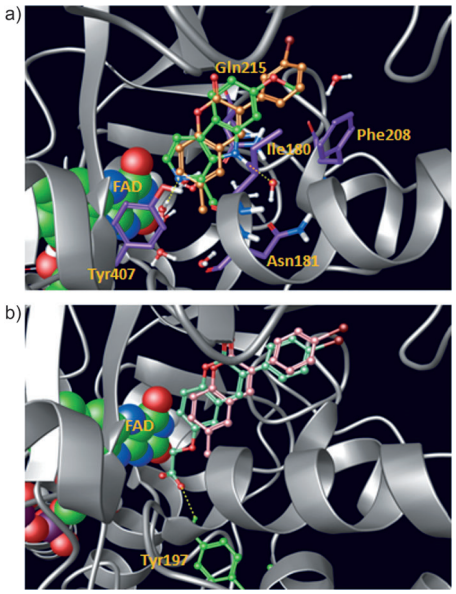

Figure 6. a) Comparison of the co-crystallized ligand harmine (colored by element, green carbon atoms) in hMAO-A (PDB: 2Z5X) and the pose retrieved by the docking calculation for compound **12** (orange carbon atoms). The ligand harmine establishes H-bond interactions with two water molecules, whereas compound **12** did not yield H-bond interactions. The residues that contribute the most to the interaction (sum of Coulomb, van der Waals, and H-bonding scores) with the ligand are colored in purple. b) Comparison of the binding modes for compounds **11** (pink carbon atoms) and **24** (aquamarine carbon atoms) in hMAO-A. The carbonyl group in the oxyacetic acid chain at position 6 of compound **24** establishes an H bond with the Tyr197 residue.

jority of the compounds were predicted to cross the BBB, according to the theoretical model. The model is very simple and explains the BBB crossing through passive diffusion without taking into account other phenomena, such as active transport mechanisms or the action of efflux pumps. Different authors developing quantitative structure–activity relationship (QSPR) models to evaluate the blood–brain partition coefficient have found the logarithm of the octanol/water partition coefficient and polar surface area to be good descriptors to explain this property.[45,50,51] In addition, we have calculated other molecular descriptors that are important in ADME properties, such as aqueous solubility. Although many drugs on the market have a log *S* value greater than −4, our compounds still present acceptable ranges of solubility with an average log *S* = −5.7. In addition, we did not find violations of Lipinski's rule (molecular weight, log *P*, number of hydrogen donors and acceptors) for almost all the compounds (23 out of 25). As MAO inhibitors have to pass different membranes and reach the CNS, this supports the potential of these derivatives as drug candidates.

From the experimental results, it can be observed that most of the tested compounds are selective inhibitors against the hMAO-B isoenzyme, with IC_{50} values in the low nanomolar and picomolar range. In fact, only compound **18** proved to be inactive against both isoenzymes. Of the 23 tested compounds, 14 presented similar or better IC_{50} values against hMAO-B than that of the selegiline (IC_{50} = 19.60 nM, reference hMAO-B inhibitor), with a much better selectivity profile. Thus, compounds **5**, **8**, **9**, **11**, **12**, **14**, and **15** proved to inhibit selectively the B isoform of the hMAO enzyme, with extremely good inhibitory activities in the picomolar range. Compound **1**, the 3-arylcoumarin skeleton, presented hMAO-B activity (IC_{50} = 11.81 μM). This was the inspiration to continue with the synthesis of new derivatives presenting this scaffold. The presence of one methyl group at position 6 (compound **2**) increased the hMAO-B activity 40-fold and maintained the excellent selectivity (IC_{50} hMAO-B = 284 nM). The presence of a methoxy group at the same position afforded compound **3**, which showed similar MAOI-B activity to compound **2** (IC_{50} hMAO-B = 413 nM). The hydrolysis of that methoxy group into a hydroxy one (compound **4**) resulted in a significant loss of activity against hMAO-B (IC_{50} = 3.39 μM). Nevertheless, compound **4** was still a better inhibitor of MAO-B than the nonsubstituted 3-phenylcoumarin (compound **1**). According to this data, derivatives substituted at position 6 were explored in the current work. According to previous work,[28–35] it was the very interesting profile of compound **9**, with a methoxy group at position 4 and a bromine atom at position 3 of the 3-aryl group, which made us have a special interest for the bromine derivatives. Also based on previous work[28–35] and the IC_{50} values of compounds **11**–**13** against the hMAO-B enzyme, the *meta* and *para* positions proved to be the most favorable points to substitute. Therefore, further experimental work was developed by taking this information into account.

Four of the most active compounds are the new coumarin derivatives **11**, **12**, **14**, and **15**, with IC_{50} values against hMAO-B between 134 and 650 pM. Compounds **11** and **12**, with different positions of the bromine atom linked in the 3-aryl ring, present a methyl group at position 6 of the scaffold. Compounds **14** and **15** have the same 3-aryl ring substitution pattern and present a methoxy group at position 6. The presence of a bromine atom in the 3-aryl ring (compounds **11** and **12**) improves the activity, relative to that with a methyl group (compounds **5** and **6**) or a methoxy group (compounds **7** and

Table 5. MM-GBSA free energy of binding and experimental/calculated pIC_{50} values for the five most active compounds in the series.[a]

Compd	hMAO-A E_{bind} [kcal mol^{-1}]	pIC_{50} obsd	pIC_{50} calcd	Compd	hMAO-B E_{bind} [kcal mol^{-1}]	pIC_{50} obsd	pIC_{50} calcd
5	−55.34	–	4.76	**5**	−66.19	9.51	7.29
11	−64.86	–	4.88	**11**	−80.10	9.41	8.23
12	−60.43	–	4.83	**12**	−82.98	9.87	8.42
14	−61.89	–	4.84	**14**	−85.57	9.49	8.59
15	−65.38	–	4.88	**15**	−82.40	9.19	8.38

[a] Calculated pIC_{50} values are provided through the respective equations calibrated for hMAO-A and hMAO-B by using the new synthesized series.

8) at the same position. So, it can be inferred that the presence of an electron-withdrawing atom (bromine atom) instead of an electron-donating group (methyl or methoxy) at those positions is an important modification to improve the activity. Based on these new results and keeping the bromine atom in the *meta* or *para* position, we decided to explore deeply the importance of the nature of the substitution at position 6. Ten new derivatives (compounds **16**–**25**) were synthesized with the aim of introducing groups with different physicochemical properties at position 6 of the coumarin moiety.

Compounds **16** and **17**, obtained by hydrolysis of the 6-methoxy derivatives **14** and **15**, showed a certain loss of activity. These compounds are still good candidates, with IC_{50} values against hMAO-B of 32 and 8 nM, respectively. Having these hydroxy derivatives as starting materials, Williamson type reactions were carried out to obtain compounds **18**–**23**. The biological results did not significantly improve, but some interesting data were found. Both the 6-(2-oxopropoxy) derivatives **18** and **21** and the 6-cyclopentyloxy derivatives **19** and **22** significantly lost the inhibitory activity and selectivity against hMAO-B. Compounds **24** and **25**, with only one carboxylic acid function on their structure, presented a very interesting activity profile, with activities against hMAO-B between 2 and 7 nM (compare with compounds **18** and **21**, respectively). Nevertheless, compound **24**, with the bromine atom in the *para* position, lost selectivity against this isoform.

In the reversibility and irreversibility tests, hMAO-B inhibition was assessed to be reversible in the presence of compound **12** (the most active compound, $IC_{50} = 134$ pM) as shown by the enzyme activity restoration after dilution of the control. However, data obtained for compound **12** showed that its degree of reversibility is lower than that described for isatin. Compound **12** was shown to be a noncompetitive inhibitor with global $r^2 = 0.97$ for the sets of Lineweaver–Burk plots constructed for the inhibition of MAO-B.

We performed docking calculations to better understand the experimental results and support the structure–activity relationship study. Based on the docking results, we have proposed a general hMAO-B binding conformation that orients the coumarin ring toward the FAD cofactor, whereas the 3-aryl ring is directed toward the entrance hydrophobic cavity. This is in accordance with the observation that small substituents at position 6 are better tolerated than bulky substituents. An increase of the size of the substituents at position 6 in compounds **18**–**25** led to a loss of hMAO-B activity. A possible cause could be the lack of space in the binding cavity, with the disruption of the proposed binding mode and possible shift of the coumarin nucleus toward the hydrophobic cavity. On the other hand, polar substituents with the ability to establish hydrogen bonds, such as hydroxy groups, could cause an opposite shift of the coumarin ring toward the FAD cofactor. This shift would cause disruption of some hydrophobic interactions between the 3-aryl ring and the hydrophobic entrance cavity. In fact, docking analysis of compounds **16** and **17** with a hydroxy substituent at position 6 showed the possibility of establishing a hydrogen bond with the FAD cofactor to be favorable for compound binding. However, this conformation could cause, at the same time, a decrease in the hydrophobic interaction contribution by the 3-aryl fragment. Similar docking results could explain the different potency shown by compounds **1** and **2** against hMAO-B (IC_{50} values of 11.81 and 0.284 μM, respectively). The docking retrieved a pose for compound **1** slightly shifted toward the FAD that could diminish the contribution of the hydrophobic interactions to the binding with the entrance cavity. However, the coumarin ring for compound **2** is placed in a very similar manner to that for compounds **12** and **14** (Figure 5), which allows a better fit for the 3-aryl ring in the hydrophobic cavity.

The 3-aryl *ortho*-bromine-substituted derivatives have experimentally shown a decrease of activity because the *meta*- or *para*-bromine-substituted compounds show a better accommodation in the hydrophobic cavity.[31] In fact, the bromine atom in the *ortho* position showed a shorter distance to the carbonyl oxygen atom of Phe168. Docking analysis suggests that polar substituents at the *ortho* position of the 3-aryl ring, such as hydroxy groups, could improve the hMAO-B activity relative to hydrophobic substituents. Compound **13** with a bromine atom in the *ortho* position showed an IC_{50} value of 4.34 μM, whereas a similar compound with a hydroxy substituent was recently reported to have an improved activity ($IC_{50} = 0.12$ μM).[31] Contrarily, polar substituents at the *meta* and *para* positions are not as appropriate for the activity as hydrophobic substitutions. This fact corroborates the information that was also recently reported by our research group.[31]

Selectivity of this type of compound toward hMAO-B has also been studied to show the ability of the compounds to recognize the pocket in hMAO-B, whereas a more limited binding has been found against hMAO-A. On one hand, compounds **11** and **12** did not show H-bond interactions with hMAO-A. On the other hand, and although compound **24** showed the capability of shifting some water molecules placed deeply in the cavity through the establishment of a hydrogen bond with Tyr197, this overall process could energetically limit the ligand–protein binding. Both isoenzymes differ in some residues in the pocket that affect selectively the binding of the studied coumarins.

Conclusions

In this study, a general and efficient synthesis of a new series of 3-arylcoumarins was developed by using Perkin, hydrolysis, and Williamson reactions. Determination of hMAO isoform activity was carried out, and the majority of the compounds exhibited selectivity for the hMAO-B isoenzyme with high affinity, in the range of nano- and picomolar concentrations. Compound **12** is more than 140-fold more active than selegiline (reference compound) against the MAO-B isoenzyme and shows advantages from the selectivity (more than 200-fold more selective than selegiline) and reversibility point of view (it is a noncompetitive inhibitor of MAO-B). Molecular docking studies were performed to establish the nature of the interaction between the studied compounds and the hMAO enzymes, which led to a rationalization of the structure–activity relationship for the synthesized series. Additionally, prediction of

blood–brain partitioning through a QSPR model showed the great potential of this type of compound to cross the BBB and act in the CNS. The results encourage further exploration of the potential of this chemical family as drug candidates for the treatment of Parkinson's disease.

Experimental Section

General methods

Starting materials and reagents were obtained from commercial suppliers (Sigma–Aldrich) and were used without further purification. Melting points (mp) are uncorrected and were determined with a Reichert Kofler thermopan or in capillary tubes in a Büchi 510 apparatus. ^{1}H NMR (300 MHz) and ^{13}C NMR (75.4 MHz) spectra were recorder with a Bruker AMX spectrometer with [D_6]DMSO or $CDCl_3$ as the solvent. Chemical shifts (δ) are expressed in parts per million (ppm) by using tetramethylsilane (TMS) as an internal standard. Coupling constants (J) are expressed in hertz (Hz). Spin multiplicities are given as s (singlet), d (doublet), dd (doublet of doublets), and m (multiplet). Mass spectrometry was carried out with a Kratos MS-50 or a Varian MAT-711 spectrometer. Elemental analyses were performed by a Perkin–Elmer 240B microanalyzer and are within $\pm$0.4% of calculated values in all cases. The analytical results are $\geq$98% purity for all compounds. Flash chromatography (FC) was performed on silica gel (Merck 60, 230–400 mesh); analytical TLC was performed on pre-coated silica gel plates (Merck 60 F254). Organic solutions were dried over anhydrous sodium sulfate. Concentration and evaporation of the solvent after reaction or extraction was carried out on a rotary evaporator (Büchi Rotavapor) operating under reduced pressure.

Synthesis

General procedure for the preparation of 3-phenylcoumarins 2, 3, 5–8, and 11–15: A solution of 2-hydroxy-5-methylbenzaldehyde or 2-hydroxy-5-methoxybenzaldehyde (7.34 mmol) and the corresponding phenylacetic acid (9.18 mmol) in DMSO (15 mL) was prepared. DCC (11.46 mmol) was added and the mixture was heated in an oil bath at 110 °C for 24 h. Ice (100 mL) and acetic acid (10 mL) were added to the reaction mixture. After being kept at room temperature for 2 h, the mixture was extracted with diethyl ether (3×25 mL). The organic layer was extracted with sodium bicarbonate solution (50 mL, 5%) and then water (20 mL). The solvent was evaporated under vacuum and the dry residue was purified by FC (hexane/ethyl acetate, 9:1).

3-(4-Bromophenyl)-6-methylcoumarin (11): White solid; yield 62%; mp: 197–198 °C; ^{1}H NMR (300 MHz; $CDCl_3$): δ = 2.44 (s, 3H; CH_3), 7.24 (dd, J = 7.9, J = 1.6 Hz, 1H; H7), 7.36 (dd, J = 7.9, J = 1.7 Hz, 2H; H5, H8), 7.56–7.62 (m, 4H; H2′, H3′, H5′, H6′), 7.78 ppm (s, 1H; H4); ^{13}C NMR (75 MHz; $CDCl_3$): δ = 20.8, 116.2, 119.2, 123.0, 127.0, 127.7, 130.1, 131.6, 132.8, 133.7, 134.3, 139.9, 151.7, 160.5 ppm; MS (EI, 70 eV): m/z (%): 317 (18), 316 (99), 315 (19) [M+H]$^+$, 314 (100) [M^+], 288 (34), 287 (22), 286 (34), 285 (17), 179 (17), 178 (36), 152 (9), 118 (14), 89 (11), 76 (12); elemental analysis: calcd for $C_{16}H_{11}BrO_2$: C 60.98, H 3.52; found: C 61.00, H 3.56.

3-(3-Bromophenyl)-6-methylcoumarin (12): White solid; yield 65%; mp: 159–160 °C; ^{1}H NMR (300 MHz; $CDCl_3$)): δ = 2.45 (s, 3H; CH_3), 7.25–7.30 (m, 2H; H7, H8), 7.36 (dd, J = 7.9, J = 2.1 Hz, 2H; H4′, H5′), 7.56 (dd, J = 7.8, J = 2.2 Hz, 1H; H6′), 7.68 (d, J = 2.0 Hz, 1H; H5), 7.80 (s, 1H; H4), 7.86 ppm (t, J = 1.8 Hz, 1H; H2′); ^{13}C NMR (75 MHz; $CDCl_3$)): δ = 20.8, 116.2, 119.1, 122.4, 127.2, 127.8, 129.9, 131.4, 131.7, 132.9, 134.3, 136.7, 140.4, 140.6, 151.7, 160.3 ppm; MS (EI, 70 eV): m/z (%): 317 (18), 316 (99), 315 (19) [M+H]$^+$, 314 (100) [M^+], 286 (34), 285 (17), 179 (17), 178 (36), 152 (9), 118 (14), 89 (11), 76 (12); elemental analysis: calcd for $C_{16}H_{11}BrO_2$: C 60.98, H 3.52; found: C 60.94, H 3.49.

3-(4-Bromophenyl)-6-methoxycoumarin (14): White solid; yield 70%; mp: 174–175 °C; ^{1}H NMR (300 MHz; $CDCl_3$)): δ = 3.88 (s, 3H; OCH_3), 6.99 (d, J = 2.8 Hz, 1H; H5), 7.13 (dd, J = 9.1, J = 3.0 Hz, 1H; H7), 7.29 (d, J = 9.1 Hz, 1H; H8), 7.54–7.60 (m, 4H; H2′, H3′, H5′, H6′), 7.79 ppm (s, 1H; H4); ^{13}C NMR (75 MHz; $CDCl_3$): δ = 55.8, 109.9, 117.5, 119.5, 119.8, 123.2, 127.5, 130.1, 131.6, 133.6, 139.8, 148.0, 156.2, 160.4 ppm; MS (EI, 70 eV): m/z (%): 333 (17), 332 (99), 331 (17) [M+H]$^+$, 330 (100) [M^+], 304 (14), 302 (14), 261 (11) 259 (11), 180 (12), 152 (55), 126 (20), 76 (11); elemental analysis: calcd for $C_{16}H_{11}BrO_3$: C 58.03, H 3.35; found: C 57.97, H 3.30.

3-(3-Bromophenyl)-6-methoxycoumarin (15): White solid; yield 72%; mp: 151–152 °C; ^{1}H NMR (300 MHz; $CDCl_3$): δ = 3.91 (s, 3H; CH_3), 7.02 (d, J = 2.9 Hz, 1H; H5), 7.17 (dd, J = 8.0, J = 2.9 Hz, 1H; H7), 7.34 (dd, J = 10.0, J = 3.9 Hz, 2H; H4′, H5′), 7.57 (dd, J = 9.8, J = 2.8 Hz, 1H; H6′), 7.70 (d, J = 7.7, 1H; H8), 7.82 (s, 1H; H4), 7.78 ppm (t, J = 1.8 Hz, 1H; H2′); ^{13}C NMR (75 MHz; $CDCl_3$): δ = 55.7, 110.0, 117.5, 119.7, 120.0, 122.5, 127.1, 127.3, 129.9, 131.4, 131.8, 136.7, 140.3, 148.1, 156.2, 160.3 ppm; MS (EI, 70 eV): m/z (%): 333 (17), 332 (99), 331 (18) [M+H]$^+$, 330 (100) [M^+], 304 (14), 302 (14), 180 (14), 152 (44), 126 (16); elemental analysis: calcd for $C_{16}H_{11}BrO_3$: C 58.03, H 3.35; found: C 58.07, H 3.40.

General procedure for the preparation of 3-(bromomethoxyphenyl)coumarins 9 and 10: A solution of 3-(methoxyphenyl)coumarins **7** or **8** (3.76 mmol), NBS (4.51 mmol), and AIBN (cat.) in CCl_4 (5 mL) was stirred and heated at reflux for 18 h. The resulting solution was filtered to remove the succinimide. The solvent was evaporated under vacuum and purified by FC (hexane/ethyl acetate, 95:5) to obtain compounds **9** and **10** in yields of 41 and 51%, respectively.[35]

General procedure for the preparation of hydroxy-3-phenylcoumarins 4, 16, and 17: A solution of substituted 6-methoxy-3-phenylcoumarin **3**, **14**, or **15** (0.50 mmol) in acetic acid (5 mL) and acetic anhydride (5 mL), at 0 °C, was prepared. Hydriodic acid (57%, 10 mL) was added dropwise. The mixture was stirred, under reflux temperature, for 3 h. The solvent was evaporated under vacuum, and the dry residue was purified by CH_3CN crystallization to yield **4**, **16**, or **17**, respectively.

3-(4-Bromophenyl)-6-hydroxycoumarin (16): White solid; yield 85%; mp: 224–225 °C; ^{1}H NMR (300 MHz; [D_6]DMSO): δ = 7.04–7.13 (m, 2H; H5, H8), 7.30 (dd, J = 8.7, J = 2.6 Hz, 1H; H7), 7.63–7.74 (m, 4H; H2′, H3′, H5′, H6′), 8.24 (s, 1H; H4), 9.82 ppm (s, 1H, OH); ^{13}C NMR (75 MHz; [D_6]DMSO): δ = 113.1, 117.3, 120.4, 120.5, 122.3, 126.1, 131.1, 131.6, 134.5, 141.4, 146.9, 154.3, 160.2 ppm; MS (EI, 70 eV): m/z (%): 319 (19), 318 (99), 317 (19) [M+H]$^+$, 316 (100) [M^+], 290 (58), 288 (60), 181 (19), 153 (12), 152 (44), 126 (15), 118 (11), 76 (14); elemental analysis: calcd for $C_{15}H_9BrO_3$: C 56.81, H 2.86; found: C 56.77, H 2.81.

3-(3-Bromophenyl)-6-hydroxycoumarin (17): White solid; yield 89%; mp: 219–220 °C; ^{1}H NMR (300 MHz; [D_6]DMSO): δ = 7.06 (t, J = 8.8 Hz, 2H; H5, H8), 7.28 (d, J = 8.9 Hz, 1H; H7), 7.42 (td, J = 8.6, J = 2.4 Hz, 1H; H5′), 7.61 (dd, J = 8.0, J = 1.3 Hz, 1H; H4′), 7.73 (dd, J = 7.8, J = 1.4 Hz, 1H; H6′), 7.93 (d, J = 1.5 Hz, 1H; H2′), 8.26 (s, 1H; H4), 9.80 ppm (s, 1H; OH); ^{13}C NMR (75 MHz; [D_6]DMSO): δ = 113.2, 117.3, 120.3, 120.6, 121.9, 125.7, 128.0, 130.7, 131.5, 131.6, 137.6,

142.0, 146.9, 154.3, 160.2 ppm; MS (EI, 70 eV): *m/z* (%): 319 (16), 318 (99), 317 (18) $[M+H]^+$, 316 (100) $[M^+]$, 290 (55), 288 (57), 181 (27) 153 (17), 152 (50), 151 (13), 126 (16), 119 (17), 76 (14), 71 (15), 69 (12), 57 (24), 55 (16); elemental analysis: calcd for $C_{15}H_9BrO_3$: C 56.81, H 2.86; found: C 56.86, H 2.90.

General procedure for the preparation of 6-(2-oxopropoxy)-3-phenylcoumarins 18 and 21: Chloroacetone (0.25 mmol) was added to a suspension of anhydrous K_2CO_3 (0.25 mmol) and the corresponding hydroxycoumarin **16** or **17** (0.13 mmol) in anhydrous acetone (3 mL). The suspension was stirred, at reflux temperature, for 16 h. The mixture was cooled and the precipitate was recovered by filtration and washed with anhydrous acetone (3× 40 mL). The solvent was evaporated under vacuum and the dry residue was purified by FC (hexane/ethyl acetate, 85:15) to obtain **18** and **21**, respectively.

3-(4-Bromophenyl)-6-(2-oxopropoxy)coumarin (18): White solid; yield 81%; mp: 157–158 °C; ^{1}H NMR (300 MHz; $CDCl_3$): δ = 2.35 (s, 3H; CH_3), 4.66 (s, 2H; CH_2), 6.98 (d, J = 2.9 Hz, 1H; H5), 7.20 (dd, J = 9.1, J = 2.9 Hz, 1H; H7), 7.30 (d, J = 9.1 Hz, 1H; H8), 7.55–7.67 (m, 4H; H2′, H3′, H5′, H6′), 7.79 ppm (s, 1H; H4); ^{13}C NMR (75 MHz; $CDCl_3$): δ = 26.6, 73.5, 111.1, 117.9, 119.8, 119.9, 123.4, 127.9, 130.1, 131.7, 133.4, 139.4, 148.6, 154.3, 160.2, 204.6 ppm; MS (EI, 70 eV): *m/z* (%): 376 (11), 375 (72), 374 (100), 373 (73) $[M+H]^+$, 372 (99) $[M^+]$, 332 (28), 331 (87), 330 (30), 329 (88), 302 (28), 301 (54), 245 (31), 164 (48), 163 (78), 152 (84), 151 (19), 126 (48); elemental analysis: calcd for $C_{18}H_{13}BrO_4$: C 57.93, H 3.51; found: C 57.87, H 3.47.

3-(3-Bromophenyl)-6-(2-oxopropoxy)coumarin (21): White solid; yield 83%; mp: 167–168 °C; ^{1}H NMR (300 MHz; $CDCl_3$): δ = 2.30 (s, 3H; CH_3), 4.61 (s, 3H; CH_2), 6.94 (d, J = 3.0 Hz, 1H; H5), 7.15 (dd, J = 9.1, J = 2.0 Hz, 1H; H7), 7.33 (dd, J = 8.1, J = 2.4 Hz, 2H; H4′, H5′), 7.53 (d, J = 9.1 Hz, 1H; H8), 7.66 (dd, J = 8.2, J = 2.3 Hz, 1H; H6′), 7.75 (t, J = 2.5 Hz, 1H; H2′), 7.83 ppm (s, 1H; H4);^{13}C NMR (75 MHz; $CDCl_3$): δ = 26.6, 73.5, 111.1, 117.9, 119.8, 119.9, 122.5, 127.2, 127.5, 130.0, 131.4, 132.0, 136.5, 139.9, 148.6, 154.3, 160.1, 204.5 ppm; MS (EI, 70 eV): *m/z* (%): 375 (20), 374 (100), 373 (21) $[M+H]^+$, 372 (100) $[M^+]$, 331 (43), 329 (43), 301 (15) 273 (10), 164 (17), 163 (31), 152 (30), 126 (13); elemental analysis: calcd for $C_{18}H_{13}BrO_4$: C 57.93, H 3.51; found: C 57.88, H 3.47.

Preparation of 6-(2-cyclopentyloxy)-3-phenylcoumarins 19 and 22: Cyclopentyl bromide (0.25 mmol) was added to a suspension of anhydrous K_2CO_3 (0.25 mmol) and the corresponding 6-hydroxycoumarin **16** or **17** (0.13 mmol) in anhydrous acetone (3.0 mL). The suspension was stirred, at reflux temperature, for 24 h. The mixture was cooled and the precipitate was recovered by filtration and washed with anhydrous acetone (3×40 mL). The solvent was evaporated under vacuum, and the dry residue was purified by FC (hexane/ethyl acetate, 9:1) to obtain **19** or **22**, respectively.

3-(4-Bromophenyl)-6-(cyclopentyloxy)coumarin (19): White solid; yield 63%; mp: 164–165 °C; ^{1}H NMR (300 MHz; $CDCl_3$): δ = 1.27–1.41 (m, 4H; 2×H3″, 2×H4″), 1.49–1.72 (m, 2H; 2×H5″), 1.77–2.29 (m, 2H; 2×H2″), 4.38 (m, 1H; H1″), 6.96 (d, J = 2.7 Hz, 1H; H5), 7.15 (dd, J = 9.1, J = 2.7 Hz, 2H; H7, H8), 7.2–7.38 (m, 2H; H2′, H6′) 7.44–7.67 (m, 2H; H3′, H5′), 7.76 ppm (s, 1H; H4); ^{13}C NMR (75 MHz; $CDCl_3$): δ = 24.0, 32.8, 80.1, 111.9, 117.5, 119.8, 120.9, 123.0, 123.1, 127.3, 130.2, 131.6, 133.7, 139.9, 147.8, 154.7 ppm; MS (EI, 70 eV): *m/z* (%): 387 (6), 386 (25), 385 (6) $[M+H]^+$, 384 (25) $[M^+]$, 319 (22), 318 (100), 317 (24), 316 (99), 290 (41) 288 (42), 181 (11), 152 (38); elemental analysis: calcd for $C_{20}H_{17}BrO_3$: C 62.35, H 4.45; found: C 62.40, H 4.49.

3-(3-Bromophenyl)-6-(cyclopentyloxy)coumarin (22): White solid; yield 65%; mp: 228–229 °C; ^{1}H NMR (300 MHz; $CDCl_3$): δ = 1.57–1.99 (m, 8H; 2×H2″, 2×H3″, 2×H4″, 2×H5″), 4.77 (m, 1H; H1″), 6.95 (d, J = 3.0 Hz, 2H; H5), 7.05 (dd, J = 8.8, J = 2.7 Hz, 2H; H7, H8), 7.24–7.35 (m, 2H; H4′, H5′), 7.53 (m, 1H; H6′), 7.76 (s, 1H; H4), 7.84 ppm (t, J = 2.0 Hz, 1H; H2′); ^{13}C NMR (75 MHz; $CDCl_3$): δ = 24.0, 32.7, 80.1, 111.9, 117.5, 119.7, 121.0, 122.5, 127.0, 127.3, 129.9, 131.4, 131.7, 136.8, 140.4, 147.8, 154.7, 160.4 ppm; MS (EI, 70 eV): *m/z* (%): 387 (11), 386 (45), 385 (12) $[M+H]^+$, 384 (45) $[M^+]$, 319 (19), 318 (100), 317 (22), 316 (100), 290 (27) 288 (27), 152 (11); elemental analysis: calcd for $C_{20}H_{17}BrO_3$: C 62.35, H 4.45; found: C 62.30, H 4.39.

Preparation of 2-[(3-phenylcoumarin-6-yl)oxy]acetyl chlorides 20 and 23: 2-Chloroacetyl chloride (0.25 mmol) was added to a suspension of anhydrous K_2CO_3 (0.25 mmol) and the corresponding 6-hydroxycoumarin **16** or **17** (0.13 mmol) in anhydrous acetone (3.0 mL). The suspension was stirred, at reflux temperature, for 24 h. The mixture was cooled and the precipitate was recovered by filtration and washed with anhydrous acetone (3×40 mL). The solvent was evaporated under vacuum, and the dry residue was purified by FC (hexane/ethyl acetate, 8:2) to obtain **20** or **23**, respectively.

2-[(3-(4-Bromophenyl)coumarin-6-yl)oxy]acetyl chloride (20): White solid; yield 63%; mp: 118–119 °C; ^{1}H NMR (300 MHz; $CDCl_3$): δ = 5.52 (s, 2H; CH_2), 7.07 (d, J = 2.5 Hz, 1H; H5), 7.19 (d, J = 8.3 Hz, 1H; H8), 7.26 (dd, J = 8.8, J = 2.4 Hz, 1H; H7), 7.60–7.72 (m, 4H; H2′, H3′, H5′, H6′), 8.20 ppm (s, 1H; H4); ^{13}C NMR (75 MHz; $CDCl_3$): δ = 89.0, 113.1, 117.2, 120.4, 122.3, 126.1, 131.0, 131.4, 131.6, 134.4, 141.3, 146.8, 154.3, 160.2, 169.0 ppm; MS (EI, 70 eV): *m/z* (%): 393 (10) $[M+H]^+$, 392 (50) $[M^+]$, 319 (14), 318 (82), 317 (15), 316 (82), 297 (11) 295 (11), 290 (42), 288 (43), 216 (13), 214 (13), 181 (16), 172 (48), 171 (26), 170 (50), 169 (24), 152 (30), 126 (24), 118 (11), 90 (20), 89 (13); elemental analysis: calcd for $C_{17}H_{10}BrClO_4$: C 51.87, H 2.56; found: C 51.79, H 2.52.

2-[(3-(3-Bromophenyl)coumarin-6-yl)oxy]acetyl chloride (23): White solid; yield 66%; mp: 157–158 °C; ^{1}H NMR (300 MHz; $CDCl_3$): δ = 5.04 (s, 2H; CH_2), 7.05 (d, J = 3.0 Hz, 1H; H5), 7.25 (dd, J = 8.0, J = 3.5 Hz, 1H; H7), 7.40 (d, J = 8.0 Hz, 1H; H8), 7.58–7.63 (m, 2H; H4′, H5′), 7.72 (dd, J = 7.6, J = 1.2 Hz, 1H; H6′), 7.91 (d, J = 1.3 Hz, 1H; H2′), 8.24 ppm (s, 1H; H4); ^{13}C NMR (75 MHz; $CDCl_3$): δ = 65.5, 112.6, 113.2, 117.3, 120.2, 120.6, 121.9, 125.7, 128.1, 130.8, 131.7, 137.6, 142.0, 146.9, 154.3, 160.2, 169.5 ppm; MS (EI, 70 eV): *m/z* (%): 393 (10) $[M+H]^+$, 392 (50) $[M^+]$, 391 (17), 390 (86), 389 (17), 388 (86), 319 (16), 318 (99), 317 (29), 316 (100), 315 (13), 290 (53), 289 (19), 288 (54), 181 (21), 153 (17), 152 (60), 126 (23), 119 (16); elemental analysis: calcd for $C_{17}H_{10}BrClO_4$: C 51.87, H 2.56; found: C 51.82, H 2.52.

Preparation of 2-[(3-phenylcoumarin-6-yl)oxy]acetic acids 24 and 25: Compounds **24** and **25** were obtained from the respective acetyl chlorides **20** and **23** in contact with the atmosphere, due to their instability.

2-[(3-(4-Bromophenyl)coumarin-6-yl)oxy]acetic acid (24): White solid; yield 100%; mp: 118–119 °C; ^{1}H NMR (300 MHz; $CDCl_3$): δ = 4.60 (s, 2H; CH_2), 7.08 (d, J = 2.7 Hz, 1H; H5), 7.21 (d, J = 8.3 Hz, 1H; H8), 7.29 (dd, J = 8.4, J = 2.6 Hz, 1H; H7), 7.64–7.75 (m, 4H; H2′, H3′, H5′, H6′), 8.22 (s, 1H; H4), 9.81 ppm (s, 1H; OH); ^{13}C NMR (75 MHz; $CDCl_3$): δ = 66.0, 114.0, 117.3, 120.9, 122.4, 126.5, 131.3, 131.5, 132.0, 134.6, 141.5, 147.0, 154.5, 160.3, 171.8 ppm. MS (EI, 70 eV): *m/z* (%): 375 (10), 374 (32) $[M+H]^+$, 373 (100) $[M^+]$, 319 (14), 181 (16), 171 (26), 126 (24), 118 (11), 90 (20), 89 (13); elemental

analysis: calcd for $C_{17}H11BrO_5$: C 54.42, H 2.96; found: C 54.43, H 2.98.

2-[(3-(3-Bromophenyl)coumarin-6-yl)oxy]acetic acid (25): White solid; yield 100%; mp: 157–158 °C; ^{1}H NMR (300 MHz; $CDCl_3$): $\delta =$ 4.83 (s, 2H; CH_2), 7.00 (d, $J = 2.9$ Hz, 1H; H5), 7.05 (dd, $J = 8.1$, $J =$ 2.8 Hz, 1H; H7), 7.25 (d, $J = 8.2$ Hz, 1H; H8), 7.36–7.43 (m, 1H; H5′), 7.57–7.60 (m, 1H; H4′), 7.70 (dd, $J = 7.8$, $J = 1.1$ Hz, 1H; H6′), 7.90 (t, $J = 1.6$ Hz, 1H; H2′), 8.23 (s, 1H; H4), 9.79 ppm (s, 1H; OH); ^{13}C NMR (75 MHz; $CDCl_3$): $\delta = 63.4$, 112.3, 114.9, 118.1, 120.8, 121.6, 122.2, 125.9, 128.4, 131.2, 132.3, 137.9, 142.5, 148.4, 155.3, 162.1, 172.3 ppm; MS (EI, 70 eV): *m/z* (%): 375 (10), 374 (32) $[M+H]^+$, 373 (100) $[M^+]$, 319 (14), 181 (16), 152 (20), 126 (23), 119 (16); elemental analysis: calcd for $C_{17}H_{11}BrO_5$: C 54.42, H 2.96; found: C 54.41, H 2.97.

Determination of the MAO isoform in vitro activity

Briefly, sodium phosphate buffer (0.1 mL, 0.05 M, pH 7.4) containing different concentrations of the test drugs (new compounds or reference inhibitors) in various concentrations and adequate amounts of recombinant hMAO-A or hMAO-B required and adjusted to obtain under our experimental conditions the same reaction velocity, that is, to oxidize (in the control group) the same concentration of substrate, 165 pmol of *p*-tyramine per min (hMAO-A: 1.1 μg protein; specific activity: 150 nmol of *p*-tyramine oxidized to *p*-hydroxyphenylacetaldehyde min^{-1} (mg protein)$^{-1}$; hMAO-B: 7.5 μg protein; specific activity: 22 nmol of *p*-tyramine transformed min^{-} (mg protein)$^{-1}$, were incubated for 15 min at 37 °C in a flat-black-bottomed 96-well microtest plate, placed in a dark fluorimeter chamber. After this incubation period, the reaction was started by adding (final concentrations) 200 μM Amplex Red reagent, 1 U mL^{-1} horseradish peroxidase, and 1 mM *p*-tyramine. The production of H_2O_2 and, consequently, of resorufin was quantified at 37 °C in a multidetection microplate fluorescence reader (FLX800, Bio-Tek Instruments Inc., Winooski, VT, USA) based on the fluorescence generated (excitation, 545 nm, emission, 590 nm) over a 15 min period, in which the fluorescence increased linearly.

Control experiments were carried out simultaneously by replacing the test drugs (new compounds and reference inhibitors) with appropriate dilutions of the vehicles. In addition, the possible capacity of the above test drugs to modify the fluorescence generated in the reaction mixture due to nonenzymatic inhibition (for example, by directly reacting with Amplex Red reagent) was determined by adding these drugs to solutions containing only the Amplex Red reagent in a sodium phosphate buffer. To determine the kinetic parameters of hMAO-A and hMAO-B (K_M and V_{max}), the corresponding enzymatic activity of both isoforms was evaluated (under the experimental conditions described above) in the presence of a number (a wide range) of *p*-tyramine concentrations.

The specific fluorescence emission (used to obtain the final results) was calculated after subtraction of the background activity, which was determined from vials containing all components except the hMAO isoforms, which were replaced by a sodium phosphate buffer solution. Under our experimental conditions, this background activity was practically negligible.

MAO activity of the test compounds and reference inhibitors is expressed as IC_{50} values, that is, the concentration of each drug required to produce a 50% decrease on the control value activity of the isoforms MAO. The corresponding IC_{50} values were calculated by using the Origin 5.0 software (Microcal Software Inc., Northampton, MA, USA), from the equations of the lines obtained by linear regression (methods least squares) of the resulting points to represent the log of the molar concentration of the test compound (*x* axis) versus the percentage inhibition of the control MAO activity achieved with corresponding concentrations of each compound (*y* axis). This linear regression was performed by using data obtained with 4–6 concentrations of each test compound capable of inhibiting the control enzyme activity of the MAO isoenzymes by between 20 and 80%. Also, the $[IC_{50(MAO\text{-}A)}]/[IC_{50(MAO\text{-}B)}]$ ratio was calculated as an indicator of the rate of selectivity in the inhibition of both isoforms.

Determination of inhibition mode

To evaluate whether compound **12** is a reversible or irreversible hMAO-B inhibitor, a dilution method was used.[43] A 100× concentration of the enzyme used in the above-described experiments was incubated with a concentration of inhibitor equivalent to 10-fold the IC_{50} value. After 30 min, the mixture was diluted 100-fold into reaction buffer containing Amplex Red reagent, horseradish peroxidase, and *p*-tyramine, and the reaction was monitored for 15 min. Reversible inhibitors show linear progress with a slope equal to ~91% of the slope of the control sample, whereas irreversible inhibition reaches only ~9% of this slope. Control tests were carried out by pre-incubating and diluting the enzyme in the absence of inhibitor.

Construction of Lineweaver–Burk plots

Sets of Lineweaver–Burk plots were constructed for the inhibition of MAO-B by a selected inhibitor, compound **12**. The initial MAO catalytic rates were measured at five different *p*-tyramine concentrations (10–1000 μM), firstly in the absence of inhibitor and then in the presence of four different concentrations of **12** (0.05–10 nM). The concentration of recombinant human MAO-B used for these measurements was 7.5 μg of protein [specific activity: 22 (nmol *p*-tyramine transformed) min^{-1} (mg protein)$^{-1}$]. All enzymatic reactions and measurements were carried out as described above. Linear regression analysis was performed by using GraphPad Prism software.[52,53]

Prediction of passive blood–brain partitioning and calculation of molecular descriptors

The procedure to calculate the theoretical log *BB* value (the logarithm of the ratio of the concentration of the compound in the brain and in the blood) was described with more detail in a previous publication.[23] We prepared the ligands with the LigPrep module.[54,55] The protonation state was established with Ionizer at pH 7. After calculating the atomic charges with the Gasteiger (PEOE) model, we calculated the topological polar surface area (TPSA) descriptors and the $\log P_{(o/w)}$ value with MOE 2011.10 software.[56] The descriptor values were introduced in Equation (1), as described by Vilar et al.,[23] in which *N* is the number of compounds used in the training set of the model developed to extract the discriminant equation, *U* is the Wilks statistic, *F* is the Fisher ratio, and *p* is the significance level.

$$\log BBclass = 0.5159 \times \log P_{(o/w)} - 0.0277 \times \mathrm{TPSA} - 0.3462 \quad (1)$$

$$N = 307 \;\; U = 0.70 \;\; F(2, 304) = 63.79 \;\; p < 0.0001$$

If the result in the equation is >0, the compounds are predicted to have a $\log BB \geq 0.3$, which means that the compounds readily cross the blood–brain barrier.[45] If the result is <0, the compounds could still cross the blood–brain barrier but with $\log BB < 0.3$. We also carried out the calculation of other molecular descriptors with the MOE 2011.10 software,[56] such as pharmacophore atom-type descriptors, atom counts, and physical properties.

Molecular docking simulations

Molecular docking simulations were carried out by using the Schrödinger 2011 package.[55]

hMAO-B

Ligand dataset preparation: The dataset was composed of 23 coumarin derivatives and different ligands belonging to hMAO-B crystal structures (PDB: 1OJ9, 1OJA, 1OJD, 2BK3, 2V5Z, 2V60, 2V61, 2XFN, 3PO7, and 4A79).[48] Different protonation states at pH 7.0 ± 2.0 by using Epik and tautomers were generated with the LigPrep module.[54] All of the structures were optimized by using the OPLS_2005 force field.

Protein structure preparation: We preprocessed the crystal structure of hMAO-B in complex with a coumarin derivative (PDB code: 2V60) by using the Protein Preparation Workflow in the Schrödinger package.[55] A water molecule establishing a hydrogen bond with the co-crystallized ligand was retained. Hydrogen atoms were added through this procedure and minimized with the OPLS_2005 force field, and heavy atoms were constrained. H-bonding optimization was carried out and included the reorientation of hydroxy groups, the water molecule, and the amide groups of Asn and Gln residues. The protonation states of His, Asp, and Glu residues were also optimized.

Receptor grid generation: A receptor grid was calculated by using a van der Waals scaling factor of 1.0 with a partial charge cutoff of 0.25. The grid was centered in the co-crystallized coumarin derivative **C17** with an outer box length of 20 Å.

QM-polarized ligand docking procedure: In the first step of the QM-polarized docking,[57] we docked the ligands to hMAO-B (PDB: 2V60) by using the Standard Precision level (SP scoring function) of Glide,[58] and three poses for each ligand were retained. Next, polarization of the ligand charges by the receptor was calculated. Quantum mechanical calculations by using Jaguar with the 6-31G*/LACVP* basis set, B3LYP density functional, and Ultrafine SCF accuracy level are carried out to determine the partial charges on the ligand atoms inside the protein pocket. In the third step, we redocked the ligands with the new charges by using the Extra Precision (XP) mode, and three poses were retained for each ligand. Ligand van der Waals scaling was 0.8. The selection of the final pose was made by taking into account the energy score (E_{model}) that combines the energy grid score, GlideScore, and internal strain energy used in the conformational search. We also analyzed binding energy values by using the Prime module.[49]

hMAO-A

A similar treatment was carried out for the hMAO-A crystal structure with the ligand harmine (PDB: 2Z5X).

Acknowledgements

This project was partially supported by personal funds of the Spanish researchers. M.J.M. thanks Fundação para a Ciência e Tecnologia for a fellowship (SFRH/BD/61262/2009). S.V. thanks the Angeles Alvariño program from Xunta de Galicia (Spain).

Keywords: coumarins · enzymes · inhibitors · oxidases · structure–activity relationships

[1] A. Cavalli, M. L. Bolognesi, A. Minarini, M. Rosini, V. Tumiatti, M. Recanatini, C. Melchiorre, *J. Med. Chem.* **2008**, *51*, 347 – 372.
[2] K. Farnikova, A. Krobot, P. Kanovsky, *J. Neurol. Sci.* **2012**, *319*, 102 – 104.
[3] M. B. Youdim, J. J. Buccafusco, *Trends Pharmacol. Sci.* **2005**, *26*, 27 – 35.
[4] P. Riederer, G. Laux, *Exp. Neurobiol.* **2011**, *20*, 1 – 17.
[5] T. Nagatsu, M. Sawada, *J. Neural Transm.* **2006**, *71*, 53 – 65.
[6] J. Bilen, N. M. Bonini, *Annu. Rev. Genet.* **2005**, *39*, 153 – 171.
[7] A. M. Cuervo, L. Stefanis, R. Fredenburg, P. T. Lansbury, D. Sulzer, *Science* **2004**, *305*, 1292 – 1295.
[8] M. Okochi, J. Walter, A. Koyama, S. Nakajo, M. Baba, T. Iwatsubo, L. Meijer, P. J. Kahle, C. Haass, *J. Biol. Chem.* **2000**, *275*, 390 – 397.
[9] M. Wimbiscus, O. Kostenko, D. Malone, *Cleveland Clin. J. Med.* **2010**, *77*, 859 – 882.
[10] K. F. Tipton, *Cell Biochem. Funct.* **1986**, *4*, 79 – 87.
[11] a) P. Dostert, B. M. Strolin, M. Jafre in *Monoamine Oxidase: Basic and Clinical Frontiers* (Eds.: K. Kamijo, E. Usdin, T. Nagausu), Excerpta Medica, Amsterdam, **1982**, p. 197; b) T. P. Singer in *Chemistry and Biochemistry of Flavoenzymes, Vol. 2* (Ed.: F. Muller), CRC, Boca Raton, **1991**, p. 437.
[12] M. V. Rudorfer, V. Z. Potter, *Drugs* **1989**, *37*, 713 – 738.
[13] a) M. Gerlach, K. Double, H. Reichmann, P. Riederer, *J. Neural Transm. Suppl.* **2003**, *65*, 167 – 193; b) H. H. Fernandez, J. J. Chen, *Clin. Neuropharmacol.* **2007**, *30*, 150 – 168.
[14] P. Riederer, W. Danielczyk, E. Grunblatt, *Neurotoxicology* **2004**, *25*, 271 – 277.
[15] L. M. Sayre, G. Perry, M. A. Smith, *Chem. Res. Toxicol.* **2008**, *21*, 172 – 188.
[16] A. M. Helguera, G. Perez-Machado, M. N. Cordeiro, F. Borges, *Mini-Rev. Med. Chem.* **2012**, *12*, 907 – 919.
[17] D. Secci, A. Bolasco, P. Chimenti, S. Carradori, *Curr. Med. Chem.* **2011**, *18*, 5114 – 5144.
[18] C. Binda, P. Newton-Vinson, F. Hubalek, D. E. Edmondson, A. Mattevi, *Nat. Struct. Biol.* **2002**, *9*, 22 – 26.
[19] C. Binda, M. Li, F. Hubálek, N. Restelli, D. E. Edmondson, A. Mattevi, *Proc. Natl. Acad. Sci. USA* **2003**, *100*, 9750 – 9755.
[20] L. De Colibus, M. Li, C. Binda, A. Lustig, D. E. Edmondson, A. Mattevi, *Proc. Natl. Acad. Sci. USA* **2005**, *102*, 12684 – 12689.
[21] C. Binda, F. Hubalek, M. Li, Y. Herzig, J. Sterling, D. E. Edmondson, A. Mattevi, *J. Med. Chem.* **2004**, *47*, 1767 – 1774.
[22] E. M. Milczek, D. Bonivento, C. Binda, A. Mattevi, I. A. McDonald, D. E. Edmondson, *J. Med. Chem.* **2008**, *51*, 8019 – 8026.
[23] S. Vilar, M. Chakrabarti, S. Costanzi, *J. Mol. Graphics Modell.* **2010**, *28*, 899 – 903.
[24] a) F. Borges, F. Roleira, N. Milhazes, L. Santana, E. Uriarte, *Curr. Med. Chem.* **2005**, *12*, 887 – 916; b) F. Borges, F. Roleira, N. Milhazes, E. Uriarte, L. Santana, *Front. Med. Chem.* **2009**, *4*, 23 – 85.
[25] a) B. Rendenbach, H. Weifenbach, H. J. Teschendorf (BASF AG), Pat. No. DE 3834861 A1, **1990**; b) F. Chimenti, D. Secci, A. Bolasco, P. Chimenti, B. Bizzarri, A. Granese, S. Carradori, M. Yez, F. Orallo, F. Ortuso, S. Alcaro, *J. Med. Chem.* **2009**, *52*, 1935 – 1942; c) D. Secci, S. Carradori, A. Bolasco, P. Chimenti, M. Yáñez, M. Ortuso, S. Alcaro, *Eur. J. Med. Chem.* **2011**, *46*, 4846 – 4852.
[26] a) A. Carotti, C. Altomare, M. Catto, C. Gnerre, L. Summo, A. De Marco, S. Rose, P. Jenner, B. Testa, *Chem. Biodiversity* **2006**, *3*, 134 – 149; b) C. Gnerre, M. Catto, F. Leonetti, P. Weber, P. A. Carrupt, C. Altomare, A. Carotti, B. Testa, *J. Med. Chem.* **2000**, *43*, 4747 – 4758.
[27] M. J. Matos, D. Viña, S. Vazquez-Rodriguez, E. Uriarte, L. Santana, *Curr. Top. Med. Chem.* **2012**, *12*, 2210 – 2239.
[28] L. Santana, F. Orallo, D. Viña, M. J. Matos, E. Quezada, M. Yañez, S. Vilar, E. Uriarte, Pat. No. ES 2343347 A1 20100728, **2010**.

[29] M. J. Matos, D. Viña, E. Quezada, C. Picciau, G. Delogu, F. Orallo, L. Santana, E. Uriarte, *Bioorg. Med. Chem. Lett.* **2009**, *19*, 3268 – 3270.
[30] M. J. Matos, D. Viña, C. Picciau, F. Orallo, L. Santana, E. Uriarte, *Bioorg. Med. Chem. Lett.* **2009**, *19*, 5053 – 5055.
[31] M. J. Matos, C. Terán, Y. Pérez-Castillo, E. Uriarte, L. Santana, D. Viña, *J. Med. Chem.* **2011**, *54*, 7127 – 7137.
[32] M. J. Matos, S. Vázquez-Rodriguez, E. Uriarte, L. Santana, D. Viña, *Bioorg. Med. Chem. Lett.* **2011**, *21*, 4224 – 4227.
[33] D. Viña, M. J. Matos, M. Yáñez, L. Santana, E. Uriarte, *Med. Chem. Commun.* **2012**, *3*, 213 – 218.
[34] M. J. Matos, D. Viña, P. Janeiro, F. Borges, L. Santana, E. Uriarte, *Bioorg. Med. Chem. Lett.* **2010**, *20*, 5157 – 5160.
[35] D. Viña, M. J. Matos, G. Ferino, E. Cadoni, R. Laguna, F. Borges, E. Uriarte, L. Santana, *ChemMedChem* **2012**, *7*, 464 – 470.
[36] G. Delogu, C. Picciau, G. Ferino, E. Quezada, G. Podda, E. Uriarte, D. Viña, *Eur. J. Med. Chem.* **2011**, *46*, 1147 – 1152.
[37] S. Serra, G. Ferino, M. J. Matos, S. Vázquez-Rodríguez, G. Delogu, D. Viña, E. Cadoni, L. Santana, E. Uriarte, *Bioorg. Med. Chem. Lett.* **2012**, *22*, 258 – 261.
[38] M. Yamada, H. Yasuhara, *Neurotoxicology* **2004**, *25*, 215 – 221.
[39] F. Hubálek, C. Binda, A. Khalil, M. Li, A. Mattevi, N. Castaganoli, D. E. Edmondson, *J. Biol. Chem.* **2005**, *280*, 16761 – 16766.
[40] S.-Y. Son, J. Ma, Y. Kondou, M. Yoshimura, E. Yamashita, T. Tsukihara, *Proc. Natl. Acad. Sci. USA* **2008**, *105*, 5739 – 5744.
[41] P. T. Prendergast, Pat. No. WO 2001003681 A2 20010118, **2001**.
[42] M. Yáñez, N. Fraiz, E. Cano, F. Orallo, *Biochem. Biophys. Res. Commun.* **2006**, *344*, 688 – 695.
[43] R. A. Copeland, *Evaluation of Enzyme Inhibitors in Drug Discovery*, Wiley-Interscience, Hoboken, **2005**.
[44] M. Gerlach, P. Riederer, M. B. Youdim, *Eur. J. Pharmacol.* **1992**, *226*, 97 – 108.
[45] D. E. Clark, *J. Pharm. Sci.* **1999**, *88*, 815 – 821.
[46] M. H. Abraham, K. Takács-Novák, R. C. Mitchell, *J. Pharm. Sci.* **1997**, *86*, 310 – 315.
[47] C. Binda, J. Wang, L. Pisani, C. Caccia, A. Carotti, P. Salvati, D. E. Edmondson, A. Mattevi, *J. Med. Chem.* **2007**, *50*, 5848 – 5852.
[48] RCSB Protein Data Bank: http://www.rcsb.org/ (accessed: June 2012).
[49] Prime ver. 3.0, Schrödinger LLC, New York, NY (USA), **2011**.
[50] G. M. Rishton, K. LaBonte, A. J. Williams, K. Kassam, E. Kolovanov, *Curr. Opin. Drug Discovery Dev.* **2006**, *9*, 303 – 313.
[51] A. R. Katritzky, M. Kuanar, S. Slavov, D. A. Dobchev, D. C. Fara, M. Karelson, W. E. Acree, Jr., V. P. Solov'ev, A. Varnek, *Bioorg. Med. Chem.* **2006**, *14*, 4888 – 4917.
[52] B. Strydom, S. F. Malan, N. Castagnoli, Jr., J. J. Bergh, J. P. Petzer, *Bioorg. Med. Chem.* **2010**, *18*, 1018 – 1028.
[53] C. I. Manley-King, J. J. Bergh, J. P. Petzer, *Bioorg. Med. Chem.* **2011**, *19*, 261 – 274.
[54] LigPrep ver. 2.5, Schrödinger LLC, New York, NY (USA), **2011**.
[55] Maestro ver. 9.2, Schrödinger LLC, New York, NY (USA), **2011**.
[56] MOE software ver. 2011.10, Chemical Computing Group Inc., Montreal, QC (Canada), **2011**: http://www.chemcomp.com/.
[57] QM-Polarized Ligand Docking protocol; Glide ver. 5.7; Jaguar ver. 7.8; QSite ver. 5.7, Schrödinger LLC, New York, NY (USA), **2011**.
[58] Glide ver. 5.7, Schrödinger LLC, New York, NY (USA), **2011**.

Received: December 16, 2013
Revised: February 28, 2014
Published online on ■■ ■■, 0000

M. J. Matos, S. Vilar, V. García-Morales, N. P. Tatonetti, E. Uriarte, L. Santana, D. Viña*

■■ – ■■

Insight into the Functional and Structural Properties of 3-Arylcoumarin as an Interesting Scaffold in Monoamine Oxidase B Inhibition

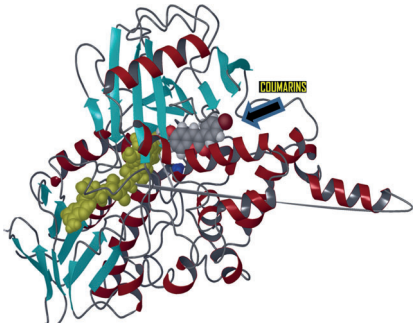

Coumarins crossing the barrier: The design and synthesis of a new series of halogenated 3-arylcoumarins are described. Monoamine oxidase A and B in vitro inhibition studies, in silico prediction of passive blood–brain partitioning, and docking calculations showed most of the 3-arylcoumarin compounds to be potent and selective.